


C.R. PHIPPS¹,
J.R. LUKE²
G.G. MCDUFF²
T. LIPPERT³

Laser-driven micro-rocket

¹ Photonic Associates, 200A Ojo de la Vaca Road, Santa Fe NM 87508, USA

² NMT/Institute for Engineering Research and Applications, 901 University Blvd. SE, Albuquerque, NM 87106–4339, USA

³ Paul Scherrer Institut, 5232 Villigen PSI, Switzerland

Received: 7 October 2002/Accepted: 8 February 2003
Published online: 28 May 2003 • © Springer-Verlag 2003

ABSTRACT We have developed a new type of miniature rocket motor for pointing and positioning microsattellites. A specially prepared tape with a transparent layer, through which the laser light passes, and an absorbing layer produce the thrust by the laser ablation process. We have achieved a specific impulse of 1800 s (greater than possible with chemistry), and laser momentum coupling coefficients of up to 50 dyn/W. The preprototype achieved 68 dyn of thrust. We discuss the target interaction physics and some of our measurements with the preprototype thruster.

PACS 42.55.Px; 42.70.Jk; 52.50.Jm; 42.62.Cf; 42.70.Km; 78.66.Qn

1 Introduction

Unknown as a field prior to 1972 [1], laser ablation propulsion is now progressing rapidly. One of the latest innovations is the micro-laser plasma thruster (μ LPT). The micro-Laser Plasma Thruster (μ LPT) is a sub-kg micro-propulsion option which is intended for attitude control and

station-keeping on microsattellite platforms. A lens focuses a laser diode beam on the ablation target, producing a miniature jet that provides the thrust. The basis for this thruster in experimental data has been reported earlier [2]. The single impulse dynamic range is nearly 5 orders of magnitude, and the minimum impulse bit is 1 nN s in a 100- μ s pulse. The laser diode that causes the ablation is a low-voltage device with an electrical efficiency in excess of 50%. The μ LPT is an alternative technology to the micro-pulsed plasma thruster (μ PPT) for micro- and nano-satellite microthrusters.

In this paper, we will emphasize the theoretical aspects of laser micropropulsion, and will discuss some results of our continuous thrust experiments.

2 Operating principles

The preprototype micro-Laser Plasma Thruster is shown in Fig. 1. The principle of operation is shown in Fig. 2. Usually, the device is operated in Transmission mode (“T-mode”) to protect optics from solid contaminants produced by the ablation jet. In this mode, a lens focuses the laser diode output on a 25- μ m diameter spot on the transparent side of a specially prepared fuel tape, creating intensities of up to 3 MW/cm² in ms-duration pulses. Passing through the acetate substrate without damaging it, the beam heats a specially pre-

 Fax: +1-505/4663-877, E-mail: crhipps@aol.com

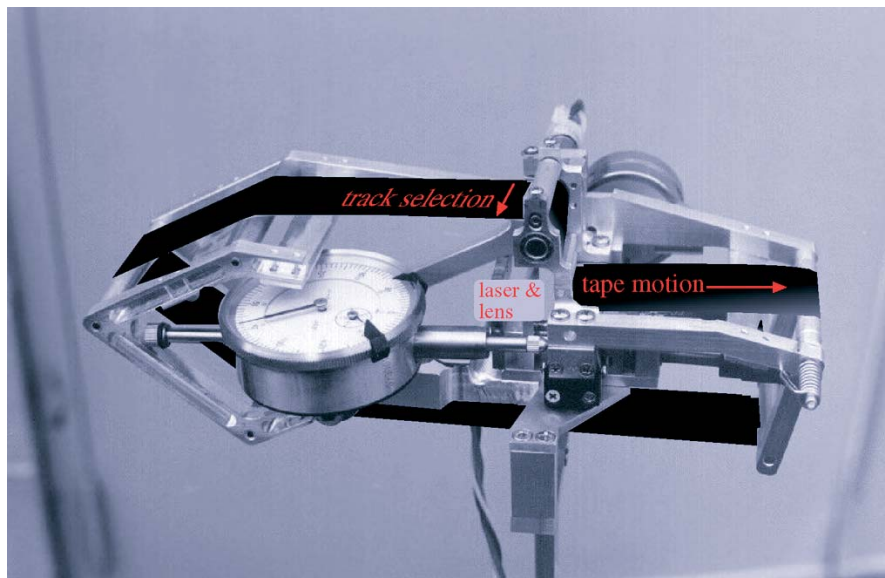


FIGURE 1 Preprototype micro-Laser Plasma Thruster built for lab tests (gauge is not part of device). Ultimate thruster will be smaller and carry more fuel

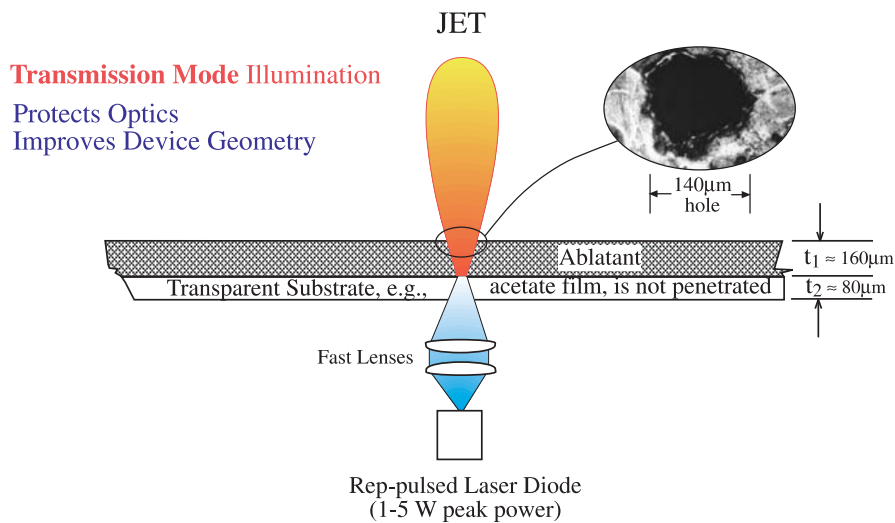


FIGURE 2 Target illumination arrangement for the μLPT

pared absorbing coating on the opposite side of the tape to high temperature, producing a miniature ablation jet. Part of the substrate facing the absorber is also ablated.

The μLPT can operate pulsed or CW, and the power density on the target can be varied by command, so operating parameters can be adjusted to match requirements. Figure 3 shows the μLPT jet in continuous operation.

The materials we have explored for the transparent substrate are cellulose acetate, PET, and KaptonTM polyimide resin. For the ablatant, over 160 materials have been studied. Many of these were so-called “designer materials” created specifically for this application [3–5]. One of these latter materials is a proprietary energetic material which generated a laser momentum coupling coefficient (see Sect. 5) of up to 50 dyn/W, about an order of magnitude larger than what is obtained from simple passive targets [6].

In continuous operation with the energetic materials, the μLPT preprototype produced a 60-dyn thrust and a specific

impulse of up to 550 s. Even with standard nonenergetic materials, the specific impulse we measured was very encouraging, and exceeded values available from chemistry [2, 7]. In single-shot tests of small samples of target material, we measured values of I_{sp} of up to 1800 s. The lifetime impulse of the prototype unit, which will contain 300 g of ablator fuel, is expected to be 160 Mdyn s. The performance of the preprototype is outlined in Sect. 5.

3 Pulsed laser–surface interactions

Pulsed lasers offer a rich parameter space in which to work compared to CW lasers. The latter have been well treated elsewhere [8]. For pulsed lasers, the momentum coupling coefficient C_m is defined as the ratio of the target momentum $m \Delta v$ produced to the incident laser pulse energy W during the ejection of laser-ablated material (the photoablation process). For continuous lasers, it is the ratio of thrust F

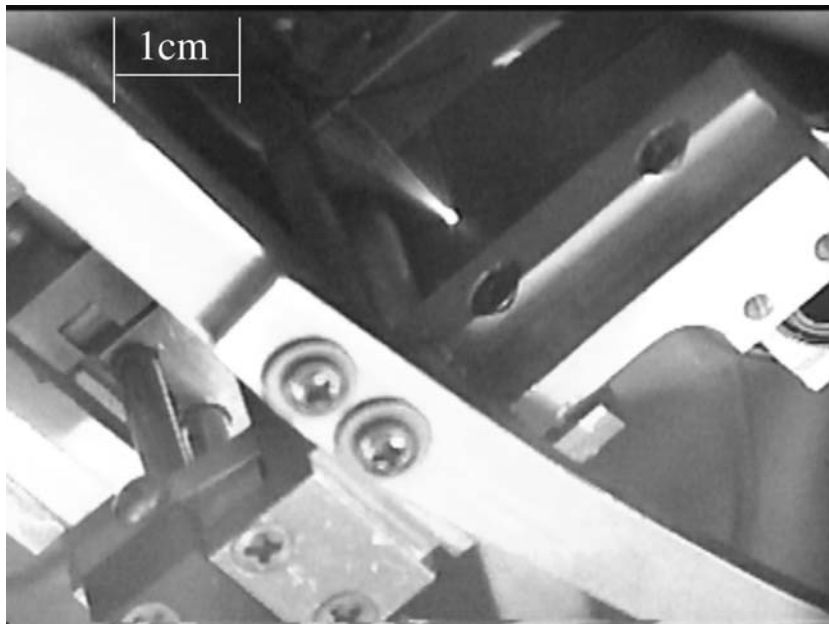


FIGURE 3 The μLPT in operation

to incident power P :

$$C_m = \frac{m \Delta v}{W} = \frac{F}{P}. \quad (1)$$

In the ablation process, Q^* joules of laser light (the asterisk is customary notation: Q^* is not a complex number) are consumed to ablate each gram of target material:

$$Q^* = \frac{W}{\Delta m}. \quad (2)$$

For the sake of discussion, we will consider a monoenergetic exhaust stream with velocity v_E . Momentum conservation requires

$$m \Delta v = \Delta m v_E, \quad (3)$$

so the product of C_m and Q^* is the effective exhaust velocity v_E of the ablation stream, independent of the efficiency with which laser energy is absorbed. This result can be seen by writing

$$C_m Q^* = \frac{(\text{dyn s})(\text{J})}{(\text{J})(\text{g})} = \frac{(\text{g})(\text{cm})}{(\text{g})(\text{s})} = \text{cm/s}. \quad (4)$$

If, for example, a significant amount of the incident energy is absorbed as heat in the target substrate rather than producing material ejection, Q^* will be higher and C_m will be proportionately lower, giving the same velocity in the end.

While it is understood that real exhaust streams have velocity distributions, we have shown [9] that the monoenergetic stream approximation will not introduce large errors ($\langle v^2 \rangle / \langle v \rangle^2 \simeq 1.15$) for laser-produced plasmas. The principal points we want to make will be easier to understand using that assumption.

The specific impulse I_{sp} is simply related to the velocity v_E by the acceleration of gravity:

$$C_m Q^* = v_E = g I_{sp}. \quad (5)$$

Energy conservation prevents C_m and Q^* from being arbitrary. Increasing one decreases the other. Using (3) and (4), energy conservation in a passive absorber requires that several constant product relationships exist:

$$2 \times 10^7 \eta_{AB} = \Delta m v_E^2 / W = C_m^2 Q^* = g C_m I_{sp} = C_m v_E. \quad (6)$$

In (6), we introduce the ablation efficiency parameter, $\eta_{AB} \leq 1$, the efficiency with which laser energy W is converted into exhaust kinetic energy. Choosing combinations of C_m and v_E that exceed 2×10^7 violates physics, since η_{AB} must be less than 1. (The constant " 1×10^7 " in (6) and (8) arises because of the mixed units in which it is customary to write C_m in the laser ablation literature (dyn/W).)

Since the maximum specific impulse of ordinary chemical rockets is about 500 s, which is limited by the temperatures available in chemical reactions, an exit velocity $v_E > 5$ km/s ($I_{sp} > 500$ s) is accessible only by laser ablation, in which temperatures can easily be many times 10 000 K, or by some other non-chemical process such as ion drives. A specific impulse I_{sp} of up to 8000 s has been measured with pulsed lasers [10].

The ablation efficiency can approach 100%, as direct measurements with other types of lasers on cellulose nitrate in vacuum verify [10], but a value of 50% or even less is likely. The impact of $\eta_{AB} < 1$ is that the C_m value deduced from a given v_E may be less than the maximum permitted by conservation of energy. The exit velocity v_E is the fundamental quantity.

The rate of mass usage is

$$\dot{m} = \frac{P}{Q^*} \text{ g/s}, \quad (7)$$

where P is the laser optical power. When considering C_m and Q^* as design variables, it must be kept in mind that the ablator lifetime τ_{AB} decreases rapidly with increasing C_m :

$$\tau_{AB} = |M/\dot{m}| = \frac{M Q^*}{P} = \frac{2 \times 10^7 \eta_{AB} M}{P C_m^2} = \frac{g^2 M I_{sp}^2}{2 \times 10^7 P \eta_{AB}}. \quad (8)$$

In (8), M is the initial mass and P is the incident laser power. For this reason, in laser propulsion applications, increasing C_m to get more thrust via the relationship

$$F = P C_m \quad (9)$$

from a given laser entails a serious penalty for the ablator lifetime, because $\tau_{AB} \propto 1/C_m^2$ from (8).

The vacuum coupling coefficient C_m is in the range 1–10 dyn/W for standard surface-absorbing materials [6].

Note that, from (6), $C_m I_{sp} \leq 2 \times 10^7 / g = 2.04 \times 10^4$. In measurements with energetic target materials, products $C_m I_{sp} = 1.8 \times 10^4$ have been obtained [10], which is 90% of 2.04×10^4 .

In the laboratory, C_m and Q^* are relatively easy quantities to measure, and their product conveniently gives v_E , which is a difficult quantity to measure, requiring, e.g., a laser-induced fluorescence setup or time-resolved shadowgraphy.

That vacuum plasma theory adapted from laser fusion [6, 11] well describes the situation above plasma threshold is now generally accepted [12, 14]. The principal results of that work which we will use here are, for the laser-initiated plasma-mediated pressure on a plane surface,

$$p_{AB} = 5.83 \frac{\Psi^{9/16}}{A^{1/8}} \frac{I^{3/4}}{(\lambda \sqrt{\tau})^{1/4}}, \quad (10)$$

and

$$T_e = 2.98 \times 10^4 \frac{A^{1/8} Z^{3/4}}{(Z+1)^{5/8}} (I \lambda \sqrt{\tau})^{1/2} \quad (11)$$

for the plasma electron temperature (in K), where $\Psi = (A/2)[Z^2(Z+1)]^{1/3}$, A is the plasma average atomic mass number, and Z is the plasma-averaged ionization state number. For coupling coefficient, (10) gives

$$C_m = 5.83 \frac{\Psi^{9/16}}{A^{1/8} (I \lambda \sqrt{\tau})^{1/4}}. \quad (12)$$

Note that (12) predicts C_m becomes very large in the limit $I \lambda \sqrt{\tau} \rightarrow 0$. This may seem counterintuitive, but one has to remember that C_m is just the ratio of a momentum to an energy

and so it varies inversely with the thermal velocity, becoming very large as $v_{th} \rightarrow 0$.

The laser intensity I should be large enough to create plasma, since the vapor regime is very inefficient, producing low I_{sp} because of the low temperature, and this puts a lower limit on $I\lambda\sqrt{\tau}$.

The plasma to vapor transition is indicated by the broad diagonal bar across Fig. 4, which shows the threshold fluence for plasma initiation and optimum coupling, based on analysis of data from 46 reports in the literature [2].

This trend is

$$\Phi = b\tau^m \tag{13}$$

or

$$I = b\tau^{m-1} \tag{14}$$

with $b = 2.4 \times 10^4$ and $m = 0.45$ for the 100 ps to 1 ms range. We would have $m = 0.50$ if the threshold for plasma formation and optimum coupling were governed by purely thermal considerations [16].

The optimum C_m for a given mission is related to the Δv for that mission. Figure 5 illustrates this dependence.

In vacuum, in the absence of gravity, the energy cost C (J/g) is given by [9]:

$$C = \frac{v_E^2}{2 \times 10^7} [\exp(\Delta v/v_E) - 1], \tag{15}$$

and the optimum (minimum) cost is given by [13]

$$\frac{\Delta v}{v_E} = 1.5936, \tag{16}$$

so that the minimum cost trend in Fig. 5 is

$$C = 1.96 \times 10^{-7} v_E^2. \tag{17}$$

In turn [9],

$$v_E = gI_{sp} \approx v_{thi} = \sqrt{2kT_i/m_i} = 9.83 \times 10^5 \sqrt{T_{i(eV)}/A}. \tag{18}$$

Figure 5 shows that large a C_m and low I_{sp} is a good choice only for low-velocity missions. When C_m is unduly high, a lot of thrust is generated per unit of laser power, but the low I_{sp} means that the fuel is depleted before the mission can be completed (see (8)). Vice versa, an engine with an unduly high I_{sp} preserves the fuel indefinitely, but has no thrust, and is useful mainly for interstellar travel. For the microthruster, Δv less than 1 m/s is the usual application, so we will emphasize high C_m and I_{sp} at the low extreme of what is possible with

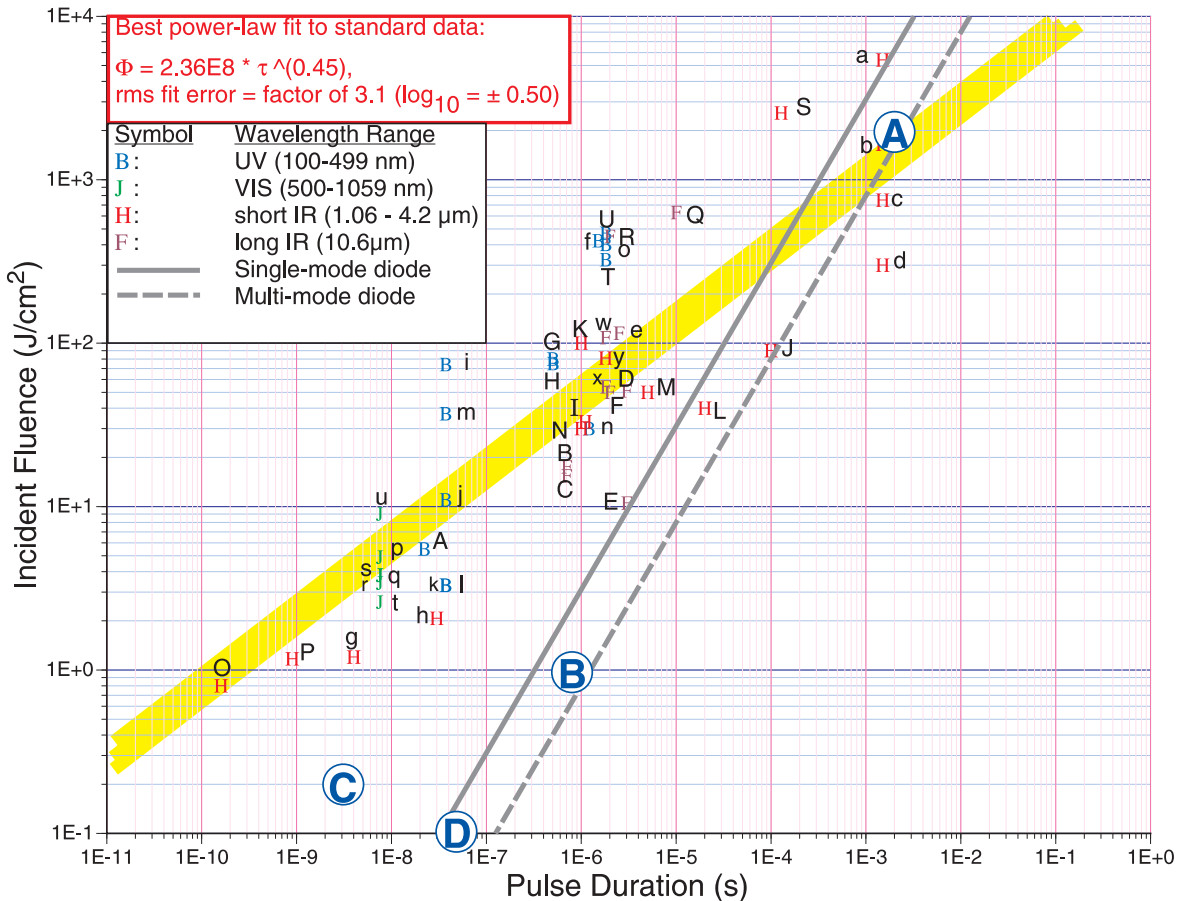


FIGURE 4 Fluence for plasma formation and optimum coupling vs. pulse duration from 46 data sets ranging from UV to IR wavelengths and pulse durations from 100 ps to 2 ms follow the (16) trend. Gray lines show intensities that are accessible by common diode lasers and focusing optics. “A”–“D” refer to operating points of experiments discussed in Table 1. Data point labels are referenced in Phipps and Luke [2]

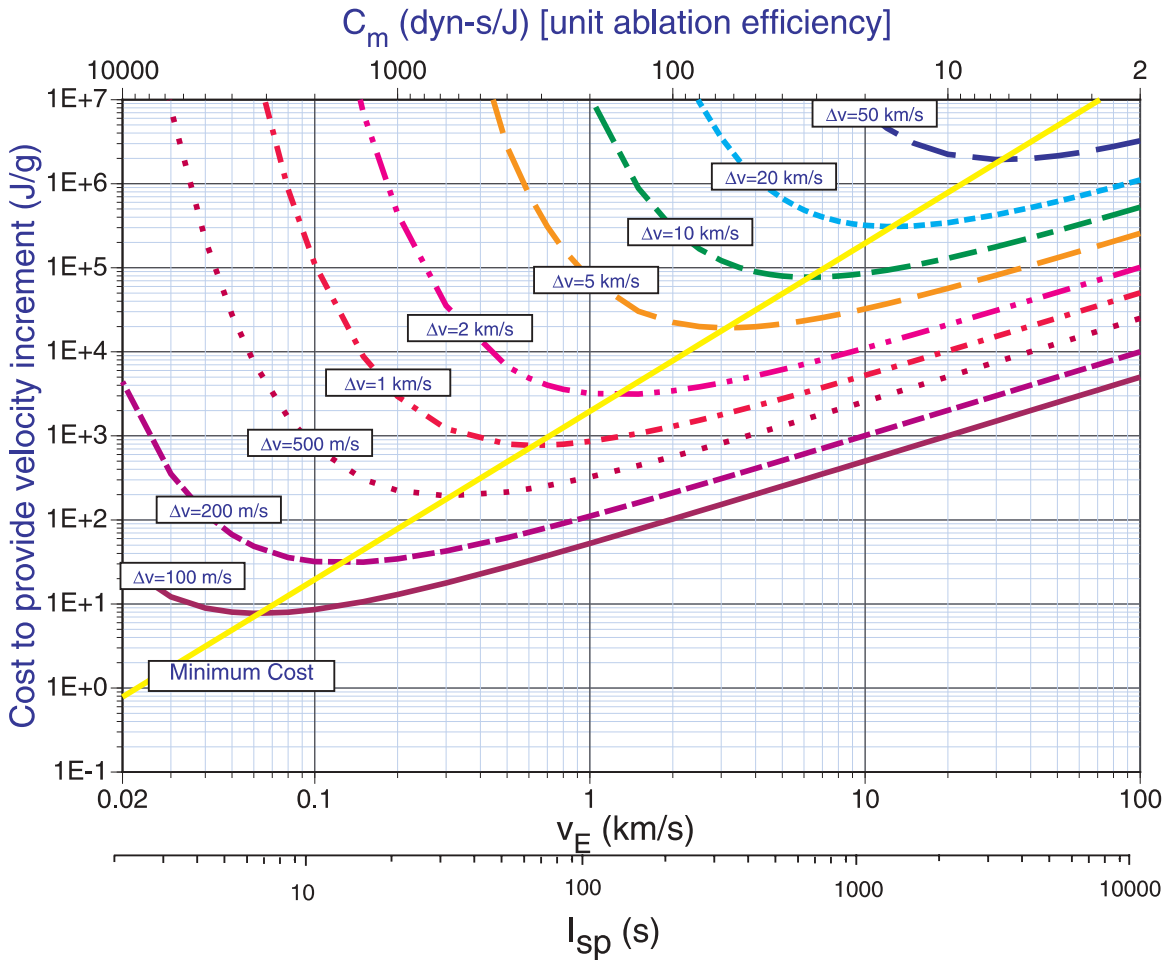


FIGURE 5 Energy cost (J/g) vs. exhaust velocity for a mission in vacuum with no gravity, for various values of Δv . The second (*lower*) horizontal axis shows corresponding values for I_{sp} , while the third (*upper*) horizontal axis shows corresponding inversely varying values of C_m , taking $\eta_{AB} = 1$

laser ablation, just slightly above the 500-s value possible with chemistry.

Table 1 gives a summary of the range of values that are found in the literature for C_m and I_{sp} . Even though I_{sp} was not measured in all cases, upper limits can be deduced from the experimental variables. I_{sp} drops precipitously as the table is descended, as does the ion temperature T_i and exhaust velocity (refer to cases “A”–“D” in Fig. 4).

4 Inducing shock in targets

Whether or not a shock is formed is an important consideration when planning to illuminate an energetic target material, to determine whether a laser-supported detonation will propagate, and in all targets to predict whether spallation will occur.

The classic analysis of high-intensity laser interaction with materials divides into two regimes: laser supported com-

Reference	Target	Laser λ, τ	Min. laser Φ (J/cm ²)	Max. C_m (dyn/W)	Max. I_{sp} (s) ^a	Min. product $I_{sp}\sqrt{\tau}$ (W \sqrt{s} /cm)
11	Simple passive (front illuminated)	various	various	10	–	0.5
This work	Proprietary energetic absorber	970 nm, 2 ms	2×10^3 “A”	52	550	4
16	Energetic absorber pyroxylin (front illuminated)	10.6 μ m, 2 μ s	5×10^6	95	200	8
17	Confined passive absorber	1.06 μ m, 85 ns	1 “B”	492	1.0	0.4
14	Confined passive absorber	1.06 μ m, 3 ns	0.2 “C”	700	(≤ 29)	0.3
18	Simulation of front-illuminated target in low-fluence limit	1.06 μ m, 50 ns	0.1 “D”	6000	(≤ 3.4)	0.05

^a Items in parenthesis are upper bounds from (6).

TABLE 1 Summary of C_m literature. “A”–“D” refer to points indicated in Fig. 4

bustion (LSC) and laser supported detonation (LSD) [17–19]. Although the analysis was originally developed by aerodynamicists for interactions in air, these concepts can also apply to a solid target in vacuum. The transition from the LSC to LSD regime is caused by laser intensities sufficient to produce a shock wave in the material, i.e., a wave velocity greater than the particle thermal velocity.

For our purposes, it is sufficiently accurate to describe shock formation by the relationship

$$\nabla p = \rho v \nabla v, \quad (19)$$

from which

$$p = \rho v^2 = \rho c_s^2. \quad (20)$$

Taking the speed of sound to be $c_s = 1 \times 10^5$ cm/s and the mass density to be $\rho = 1$ g/cm³, we find a laser-induced pressure of $p \simeq 1 \times 10^{10}$ dyn/cm² = 10 kbar is necessary to produce a shock. The energy density involved is

$$u = \frac{3}{2}nkT = \frac{3}{2}p = \frac{3}{2}(1 \times 10^{10}) \text{ erg/cm}^3. \quad (21)$$

In practical terms, $u = 1500$ J/cm³. (10) gives the combination of laser intensity I (W/cm²), pulsewidth τ (s), and wavelength λ (cm) that will give the required pressure. Without much loss, we can take $\Psi = 1$ and, for a carbon-hydrogen plasma, $A = 6$ in (10) and (11). Table 2 uses these values to illustrate the order of magnitude of pressure predicted by (10) during a laser pulse which is front-illuminating a standard material target in vacuum at $\lambda = 970$ nm.

Pulse duration	Conditions	Intensity I	Pulse energy W	Pressure (bar)
4 ms	μ LPT parameters	13 kW/cm ²	4 mJ	0.43
10 ns	Approaching laser fusion	5.9 GW/cm ²	1800 J	10 k

TABLE 2 Laser-induced pressure vs. laser parameters

In other words, it requires conditions approaching those of laser fusion in an unconfined target to create a propagating detonation in the target. In a confined (layered) target, on the other hand, it takes far less laser intensity. Fabbro et al. [14] have shown pressure amplification of up to a factor of 70 by confining the plasma between an anvil and a glass plate through which the laser light is introduced to the target. Other workers have replaced the glass plate with a liquid film for industrial applications [20]. Nevertheless, for the pulse durations we plan for the μ LPT, shock formation is highly unlikely.

5 Progress with the preprototype thruster

5.1 Operating parameters

Since our previous report on this work [21], considerable progress has occurred.

Table 3 shows the parameters for the “preprototype” microthruster that we have developed, including the expected

Parameter	PVC ablatant	Energetic ablatant
Weight with fuel (g)	850	850
Tape dimensions (cm \times cm \times μ m)	50.5 \times 2.54 \times 240	50.5 \times 2.54 \times 240
Laser wavelength (nm)	970	970
Peak laser power ^a (W)	6.25	15
Average laser power (W)	1	2.4
Laser focal spot diameter (μ m)	25	25
Tape speed (mm/s)	20	20
Pulse duration τ (ms)	2	2
Pulse duty factor	0.16	0.16
Pulse repetition frequency (Hz)	80	80
Track width, normal operation (μ m)	100	100
Tracks	254	254
Tape lifetime (h)	1	3.5
Coupling coefficient C_m (dyn/W)	7	30
Pulse fluence on target Φ (kJ/cm ²)	2.6	6.1
Pulse intensity on target I (MW/cm ²)	1.3	3.1
Force output (dyn)	7	70
Lifetime impulse J_{tot} (kdyn s)	25	880
Q^* (kJ/g)	13	13
I_{sp} (s)	200	400
Minimum impulse bit (dyn s)	0.1 ^b	0.1 ^b
Maximum laser heatsink temperature ($^{\circ}$ C)	80	80

^a with fiber-coupled diode lasers.

^b at 1 ms pulsewidth.

TABLE 3 Typical operating parameters for the μ LPT preprototype

behavior when the energetic fuel tapes are used. We determine thrust in vacuum with a torsion balance [2], which can measure 5 dyn with 10% accuracy. Its force response is 500 dyn/rad.

In most cases, two types of ablatant have been used for this work. The first is carbon-doped polyvinylchloride (PVC). Its performance is shown in the middle column of Table 3 and in Fig. 6. Its advantages are ease of preparation, and adequate performance for our application. Its main disadvantages are significant outgassing (up to 1% $\Delta m/m$ per hour) and undesirable emission of carbonaceous contaminants at large angles from the μ LPT jet.

The second is a proprietary energetic material developed by one of the authors at the Paul Scherrer Institut. Its performance is shown in column 3 of Table 3 and in Fig. 7. This data plot clearly shows a sharp threshold for thrust production in the energetic material. The material releases 3.1 kJ/g on thermal decomposition and has a molecular weight of around 5 kg/mol.

Control of, and communication with, the thruster in the vacuum chamber is through a universal asynchronous receiver transmitter channel and an onboard Texas Instruments MSP430 microcontroller. The MSP430 was chosen for its ultra low power, only 7 mW at full computing speed and only 5 μ W in standby. The total mass for the microcontroller is about 2.2 grams.

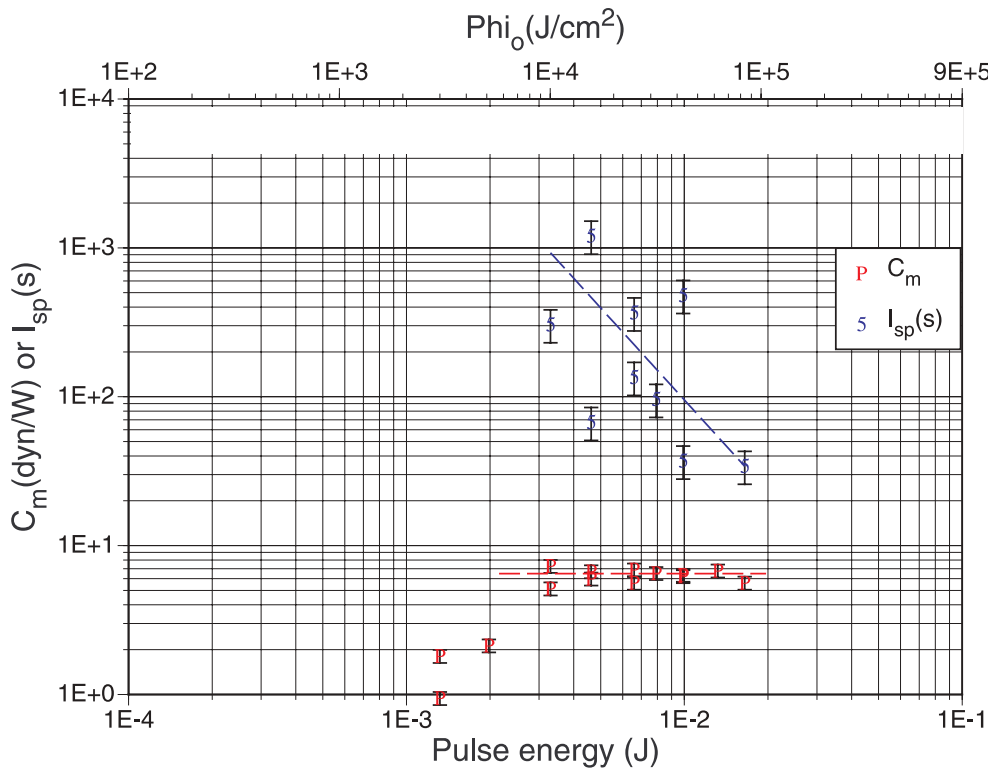


FIGURE 6 Coupling coefficient and specific impulse measured with single pulses from the single-mode research laser focused to a 5- μm spot diameter, on a standard PVC/acetate target material in T mode. Note the nearly constant C_m value of 6.2 dyn/W above threshold. A specific impulse I_{sp} in excess of 1000 s was seen

Data Sets ID66*
 Coating: Scherrer Energetic 370 μm
 Substrate: Kapton 80 μm

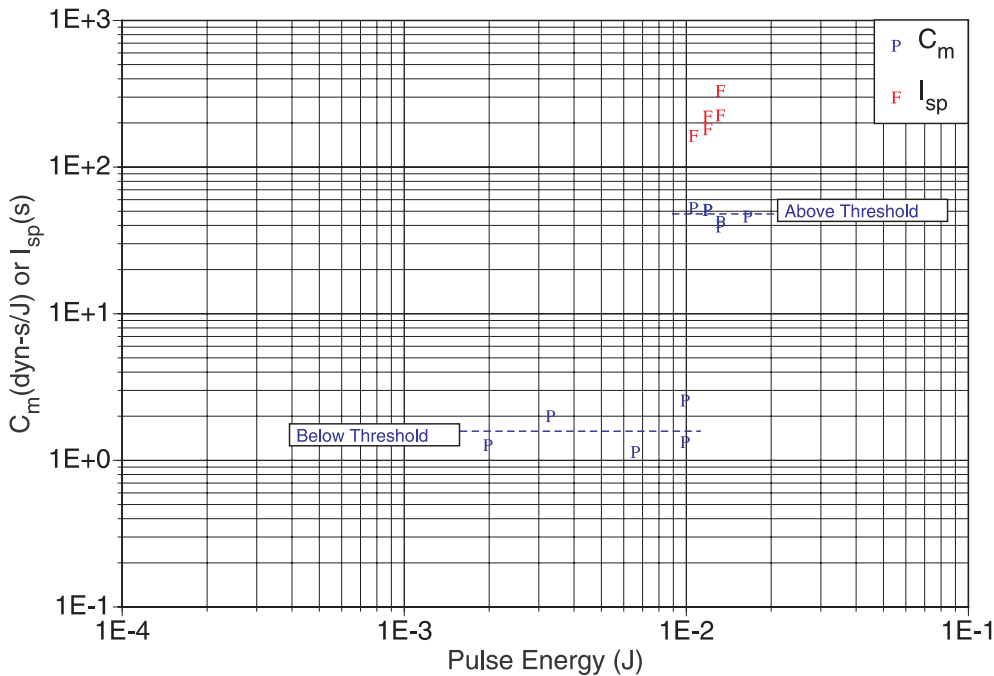


FIGURE 7 This data plot clearly shows the threshold for the energetic material. In other measurements, values of C_m as large as 50 dyn/W (500 $\mu\text{N/W}$) and I_{sp} up to 550 s were obtained with proprietary energetic μLPT fuel, together with a maximum product $C_m I_{sp} = 16870$. This number is equivalent to 83% of the theoretical maximum for a perfectly efficient *nonenergetic* absorber, and implies an exhaust velocity of 5.4 km/s

5.2 μLPT operation

We have made tapes from several of the ablatant/substrate combinations identified in the static impulse tests and tested their performance using the “preprototype” continuous thrust test device.

To measure thrust, we use a sensitive torsion pendulum that suspends the thruster and its electronics [2]. The pendulum is calibrated using a crossed pair of Helmholtz coils. A large field coil is attached to the support frame, and a small armature coil is attached to the pendulum, which is oriented perpendicular to the field coil. By applying current to the coils,

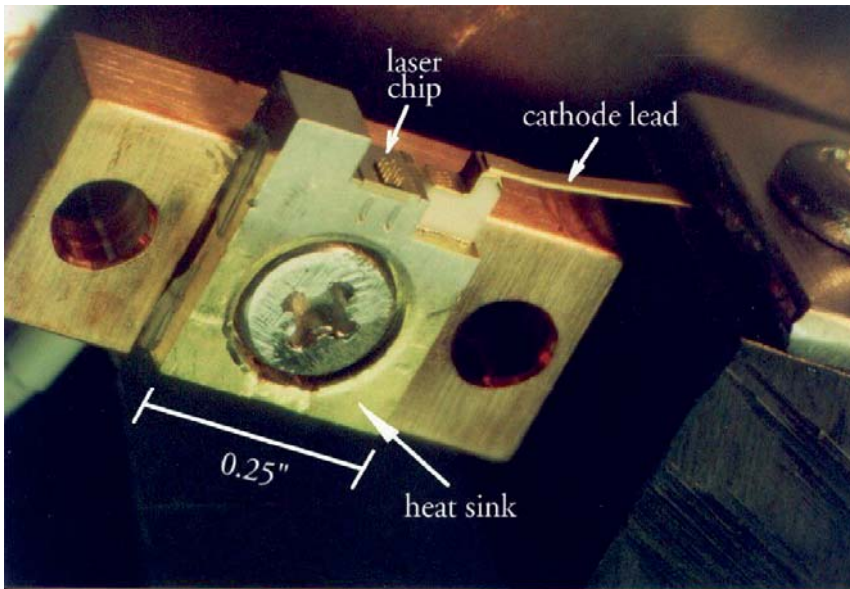


FIGURE 8

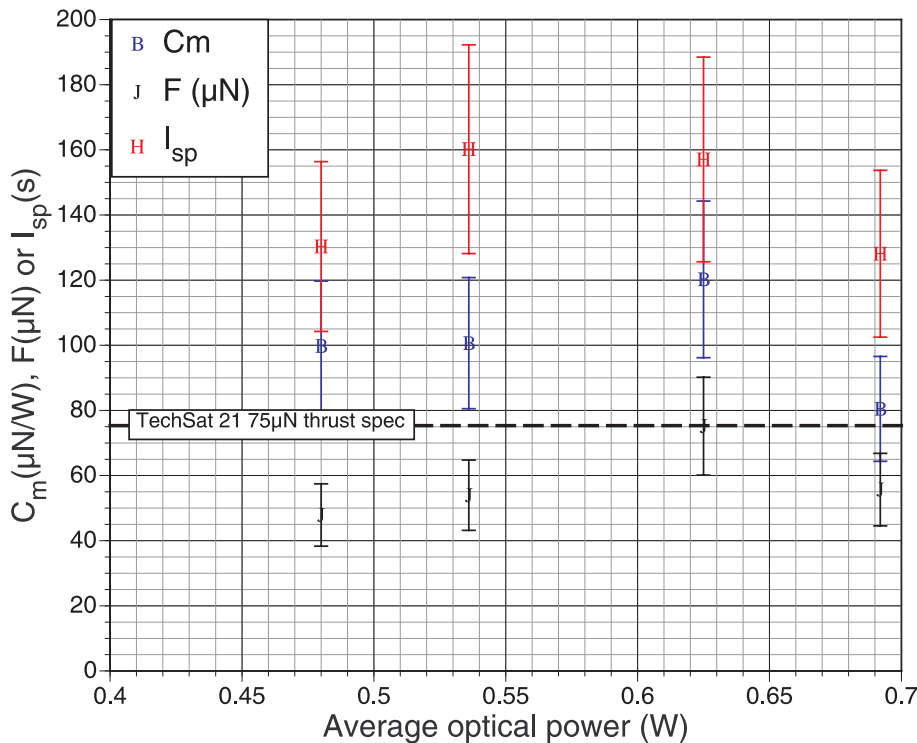


FIGURE 9 First measurements of thrust, thrust-to-power ratio, and specific impulse for the preprototype in low-power tests

a small well-defined torque can be applied to the pendulum and its response measured. The field coil produces a magnetic field much larger than the local horizontal component of the Earth's field.

We always operate the μLPT preprototype in the repetitively pulsed mode, because we found that the moving tape steers the μLPT jet unacceptably in the CW mode [22]. During a ms-duration pulse, however, tape motion is negligible and the plume is well-defined (Fig. 3) and perpendicular to the tape. This change brought with it three benefits: operation in closer contact with the bulk of our static test data (which is pulsed data), operation at a higher peak power for a better I_{sp} ,

and low duty factor operation of our laser diodes, which is better for their heat dissipation. It also brought a difficulty: the low duty factor requires us to use more diodes for the same average power and thrust. This requirement will have only a minor impact on the weight of the microthruster unit. (Fig. 8 shows the very small size of the lasers involved.)

The combination of Φ and τ used in the preprototype puts us well into the plasma regime (point "A", Fig. 4).

Figure 9 shows measurements of thrust using standard (non-energetic) target materials at low laser power. Other thrust measurements have been made and will be reported in the future.

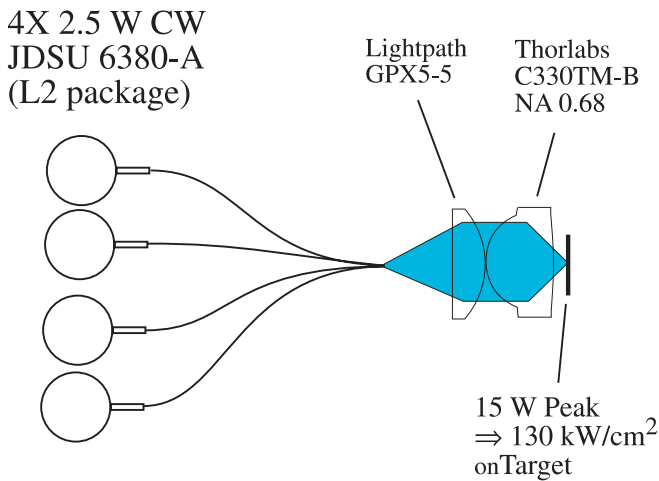


FIGURE 10 High-power laser-illumination scheme images optical fibers on target at high peak power

For these tests, four JDSU 6380-A fiber-coupled, 920-nm diodes (Fig. 10) deliver up to 15-W peak power (3-W average) to the target in a tightly focused spot.

The μ LPT prototype thruster will incorporate advances in performance developed with the preprototype and, instead of 50 cm of fuel tape, will incorporate 300 g of expendable fuel in an 80-m \times 2.54-cm tape, enabling it to generate an impulse of 160 Mdyns over its 750-hour lifetime. This is sufficient to de-orbit or significantly raise the orbit of a microsatellite, in addition to serving the primary function of attitude control for which the μ LPT is designed.

6 Summary

A new type of microthruster has been developed which is an alternative to the μ PPT for spacecraft microthrusters. The μ LPT is one of the first practical applications of laser ablation propulsion. When complete, the μ LPT prototype will exceed all Air Force requirements for TechSat21-type microthrusters.

Laser-surface interaction theory shows that the combination of coupling coefficient C_m and specific impulse I_{sp} developed by this thruster is appropriate for its mission.

ACKNOWLEDGEMENTS This work was completed with support from AFOSR Contract No. F49620-00-C-0005.

REFERENCES

- 1 A. Kantrowitz: *Aeronaut. Astronaut.* **10**, 74 (1972)
- 2 C. Phipps, J. Luke: *AIAA J.* **40**, 310 (2002)
- 3 T. Lippert, C. David, M. Hauer, A. Wokaun, J. Robert, O. Nuyken, C.R. Phipps, S. Langford, J. Dickinson, U. Kogelschatz: *J. PCB*, 145 (2001)
- 4 T. Lippert, C. David, M. Hauer, T. Masubuchi, H. Masuhara, O. Nuyken, C. Phipps, J. Robert, T. Tada, K. Tomita, A. Wokaun: *Appl. Surf. Sci.*, 13 (2002)
- 5 T. Lippert, C. David, M. Hauer, C. Phipps, A. Wokaun: *Rev. Laser Eng.* **29**, 734 (2001)
- 6 C. Phipps, T. Turner, R. Harrison, G. York, W. Osborne, G. Anderson, X. Corlis, L. Haynes, H. Steele, K. Spicochi, T. King: *J. Appl. Phys.* **64**, 1083 (1988)
- 7 C. Phipps, J. Luke, G. McDuff: 'A Diode-Laser-Driven Microthruster'. In: *Proc. Int. Electr. Propul. Conf. in Pasadena, 2001*, paper IEPC-01-220
- 8 P. Loosen: *Proc. SPIE* **1810**, 26 (1993)
- 9 C. Phipps, J. Reilly, J. Campbell: *J. Laser Part. Beams* **18**, 661 (2000)
- 10 C. Phipps, M. Michaelis: *J. Laser Part. Beams* **12**, 23 (1994)
- 11 C. Phipps, R. Dreyfus: 'Laser ablation and Plasma Formation'. In *Laser Ionization Mass Analysis*, ed. by A. Vertes, R. Gijbels, F. Adams (Wiley, New York 1993)
- 12 A. Saleres, B. Cazalis, P. Combis, J. David, B. Meyer, G. Nierat, S. Sibille, G. Thiell, F. Wagon: 'Couplage thermique et mécanique dans l'interaction laser-matière à éclairnement modéré'. In *Revue Scientifique et Technique de la Défense*, CEL-Valenton report 77 (1992)
- 13 W. Möckel: *J. Spacecraft Rockets* **12**, 700 (1975)
- 14 R. Fabbro, J. Fournier, P. Ballard, D. Devaux, J. Virmont: *J. Appl. Phys.* **68**, 775 (1990)
- 15 C. Phipps Jr., R. Harrison, T. Shimada, G. York, T. Turner, X. Corlis, H. Steele, L. Haynes, T. King: *Laser Part. Beams* **8**, 281 (1990)
- 16 H. Carslaw, J. Jaeger: *Conduction of Heat in Solids*, 2nd edn. (Clarendon Press, Oxford 1959) pp. 75-76
- 17 A. Pirri: *Phys. Fluids* **16**, 1435 (1973)
- 18 A. Pirri, R. Root, P. Wu: *AIAA J.* **16**, 1296 (1978)
- 19 Y. Raizer: *Laser-Induced Discharge Phenomena* (Consultants Bureau, New York 1977) pp. 198-249
- 20 P. Peyre, R. Fabbro, L. Berthe, X. Scherpereel, E. Bartnicki: *Proc. SPIE* **3343**, 183 (1998)
- 21 C. Phipps, J. Luke: *Proc. SPIE* **4065**, 801 (2000)
- 22 J. Luke, C. Phipps, G. McDuff: 'Laser Plasma Thruster Continuous Thrust Experiment', paper 4760-105, *Proc. SPIE* **4760**, 843 (2002)